Preparation and Investigation Physical Properties of Functionally Graded Materials of Aluminum-Nickel Alloys

To cite this article: Massoud Aziz Hussein *et al* 2021 *J. Phys.: Conf. Ser.* **1999** 012067

View the article online for updates and enhancements.

Preparation and Investigation Physical Properties of Functionally Graded Materials of Aluminum-Nickel Alloys

Massoud Aziz Hussein[1], Saad Hameed Al-Shafaie[2] and Nabaa S. Radhi[2]

massoud.aziz85@gmail.com

[1]Iraqi Ministry of Interior

[2]University of Babylon/ Collage of Materials Engineering

Abstract Materials that are functionally graded and have a layered structure made of nickel and aluminum were fabricated by powder metallurgy procedure. Al/Ni FGM consist of five layers. The functionally graded material sample starts with pure aluminum and ends with pure nickel. the graded layers were (25 Ni-75Al) %, (50 Ni-50 Al) % and (75 Ni-25Al) %. Samples were sintered at a temperature 600° C. Apparent density, green density, porosity, and shrinkage of each layer were measured.

Keywords: Functionally graded materials, aluminum-nickel alloy, powder metallurgy, apparent density and porosity, green density

1. Introduction

Functionally Graded Materials are those in which the composition and structure change gradually, causing the material's properties to change [1]. Gradients of phase distribution, porosity, texture, structure, and other related properties (hardness, resistance, thermal conductivity, density, Young's modulus, etc.) distinguish them among isotropic materials. The presence and appearance of compositional or other gradients, as well as the sophisticated behavior of FGM components, distinguishes the FGM from conventional (macroscopically uniform) materials [2-4]. Functionally graded materials are all over the place in nature. FGM can take many forms, including human skin, bone, or the bamboo tree. These are the most advanced materials in the engineering composites family, which are made up of two or more constituent phases with a continuously and smoothly changing composition [5]. Due to compositional variations within each layer, non-uniform density gradients in the green body of a FGM made by powder compaction can cause non-uniform shrinkage during sintering [6,7]. These materials (Al/Ni alloy) have been used in the fields of aircraft, space shuttle and automobiles, due to their important and vital role in developing these fields [8]. In this study the physical properties of the layers of (Al/Ni) FGM such as apparent density, porosity and green density were studied additionally the apparent density of Al and Ni powders. Particle distribution and particle size of Ni and Al powder are determined. There has been a lot of research work performed on the study of FGM in the literature. Mandira Bhattacharyya et al fabricated and designed aluminum–silicon carbide (Al/SiC) and nickel–alumina (Ni/Al$_2$O$_3$) and they studied the microstructure and the content of porosity and hardness are also determined [9]. S. Vijay et al. investigated the stiffness and compressive strength of a nickel-reinforced B$_4$C coated 601AC / 201AC

material with selective functional gradient layers in a comparative study. Powder metallurgy (P/M) is used to create FGM samples of two, three, or five layers [10].

Aim of this work, measured and studied apparent density, green density, porosity, and shrinkage of functionally graded materials (Al-Ni) and each layer in these materials.

2.Experimental details
2.1 FGM preparation

FGMs is made from mixtures of powders containing different volume fractions of Al and Ni. The nickel powder had an average particle size of 9.922 μm and the aluminum powder had an average particle size of 18.3μm. All of the layers made use of these powders. Cold-pressed (CP) uniaxially mixed powders for each layer at 800 MPa in a round steel of 10 mm in diameter. Using the vacuum furnace, for 3 hours, a maximum sintering temperature of 600° C was maintained at a rate of 10ºC/min. After that, the furnace was turned off to bring it to room temperature. In this work the functionally gradient materials of aluminum and nickel were fabricated in five layers. The first layer was made of pure aluminum, with a height of 3 mm. Volume fractions and the height of the gradient layers were: the second layer was (25 Ni-75Al) % and a height of 2.5 mm, for the third layer was (50 Ni-50 Al) % and a height of 2 mm and for the fourth layer was (75 Ni-25Al) % and a height of 1.5 mm. the fifth layer was made of pure nickel, with a height of 1 mm. The Fig. (1) shows the Al/Ni FGM sample after mixing (for 30 minutes) and pressing.

Figure 1. (Al/Ni) FGM sample after mixing and pressing.

2.2 Particle size and particle distribution

Particle size analyzer type (Bettersize2000 laser particle size analyzer) was used to determine the particle size of Ni and Al powder used in the current research.

2.3 Apparent density of elemental and blended powders

Filling the powder into a regular graded cup with a maximum volume of 10 mL into an appropriate grade is used to determine apparent density. A microbalance is used to determine the weight of the cup

with and without powder, with an accuracy of ± 0.001 grams. The apparent density is calculated using the following equation [11].

$$\rho_A = \frac{m_2 - m_1}{V_p} \ldots \ldots \ldots \ldots (1)$$

Where:

ρ_A: the powder's apparent density (g/cm³) , m_1: cup weight (without powder) (cup empty) ,
m_2: the weight of the cup while it is filled with powder, V_p: powder volume in a cup (cm³).

2.4 Green density and Porosity of FGM compacts

G D is the ratio of powder metal volume to the external of the external volume. It is computed as follows using dimension evaluations and compact sample weighing [11].

$$\rho_g = \frac{m_g}{V_g} \ldots \ldots \ldots \ldots (2)$$

Where: ρ_g: green density (g/cm³) , m_g: the compact's green mass (g), Vg = volume of the compact (cm³).

Green porosity is calculated using the Bragg – Kleeman rule, determined as follows: the theoretical density multiplied by the weight percent of each elemental powder

$$\rho_{tB} = \sum_{i=1}^{n} Wt_1 * \rho_1 + Wt_2 * \rho_2 + Wt_3 * \rho_3 + \cdots \cdots \cdots + Wt_n * \rho_n \cdots \cdots \cdots \cdots \cdots (3)$$

Where ρ_{tB}: theoretical density of blended powder (g/cm^3), n= No. of elemental powders,
Wt= weight percent (%) ,$\rho_{1,2,3\ldots n}$ = density of elemental powder. As a result, the green porosity is dimensionless quantity determined by using the following equation:

$$P_g = \left(1 - \frac{\rho_g}{\rho_{tB}}\right) * 100\% \cdots \cdots \cdots (4)$$

Where P_g= green porosity (%),ρ_g= green density (g/cm^3), ρ_{tB} = calculated density of blended mixture (g/cm^3).

2.5 Apparent density and porosity of sintered compacts

Standard methods such as micrometers and calipers cannot accurately measure the volume of arbitrary powder metallurgy products. The precise method to measure the volume of water displaced by immersed objects is determined by the Archimedes principle, since density is a mass/volume. A method to seal surface connected pores is required for porous powder metallurgy parts. If the pores aren't sealed or the port isn't oil-impregnated, the region can absorb some of the water, lose buoyancy, and have an incorrectly high density. ASTM-B 328-96 is used to measure the density and porosity of sintered portions [13]:

1- The sample is dried at 100°C in an argon atmosphere for 24 hours before being cooled to room temperature. The dry sample's weight is expressed as mass A.

2- At room temperature, using a suitable evacuating pump, the pressure was reduced over the immersed specimen in oil with viscosity 22 cst at 37°C for less than (7kPa) pressure for 25 min.

3- The weight of the completely impregnated sample in air was determined to be B.

4- In water, weigh the specimen that has been completely impregnated (Mass F)

5- Take temperature readings to determine the density of water at this temperature. For this research, the temperature was 21°C, and at this temperature, the water density (Dw) was 0.99802 gram / cm³, the following equation is used to calculate density (D).:

$$D = \left(\frac{A}{B-F}\right) * D_w \cdots\cdots\cdots (5)$$

and the porosity can be measured by

$$P = \left[\frac{B-A}{(B-F)*D_o}\right] * D_w \cdots\cdots\cdots (6)$$

Where Do : density of oil = 0.963 g/cm³

2.6 Changes in the dimensions of sintered samples
The sintered compact specimen's dimensional change is determined using the equation below. [13].

$$\textit{Dimensional change } (\%) = \frac{D_S - D_D}{D_D} * 100 \cdots\cdots\cdots (7)$$

Where DD: mold cavity diameter (mm), Ds: the sintered sample diameter (mm).

3-Results and Discussion
3.1 Particle size and distribution of powders
Particle size and its distribution for both the powders (Al and Ni) were measured using the particle size analyzer, and the accumulative plot for each powder is shown in figures (2) and (3). It is clear that the particle size of (Ni and Al) are (9,922 and 18,3 μm) respectively. The apparent density of a particle decreases as its size decreases because the powder's specific surface area is greater for smaller particles which the friction between particles increases, and the apparent density decreases subsequently [11]. On the other hand, most powders used for compaction have an irregular shape. The addition of fine spherical powder such as powder Ni increases apparent density while the addition of powdered flake decreases the apparent density [14]. The percentage of particles between the coarsest and finest particles, as well as their relative amounts, determine apparent density. Different particle size ranges are selected for good compacts as well as good sintered product properties [11].
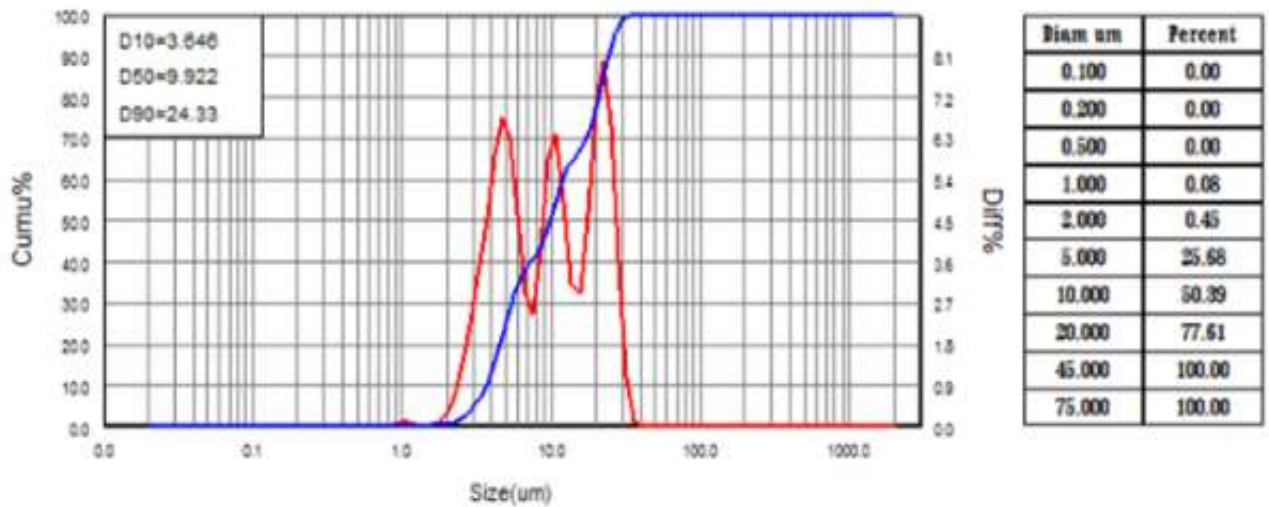
Diam um	Percent
0.100	0.00
0.200	0.00
0.500	0.00
1.000	0.08
2.000	0.45
5.000	25.68
10.000	50.39
20.000	77.61
45.000	100.00
75.000	100.00

Figure 2. particle size analysis for Ni powder**.**

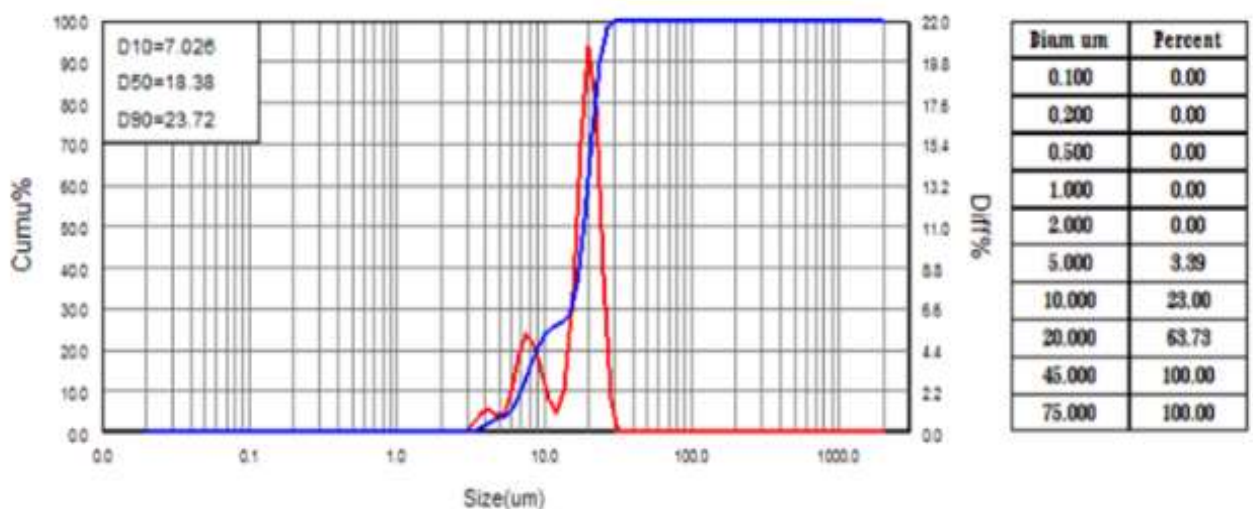| Diam um	Percent
0.100	0.00
0.200	0.00
0.500	0.00
1.000	0.00
2.000	0.00
5.000	3.39
10.000	23.00
20.000	63.73
45.000	100.00
75.000	100.00

Figure 3. particle size analysis for Al powder**.**

3.2 Elemental and mixed powders' apparent density

Apparent density of elemental powders used to create a blended mixture of alloys has been measured and illustrated in figure (4). When compared to Aluminum and FGM, Nickel has the highest apparent density.

Figure (4) shows that the apparent density of the FGM sample is almost in the center of the apparent density values of aluminum (2.5 g/cm³) and nickel (6.82 g/cm³). The apparent density of a metal powder is based on the total density of the material, particle size and its distribution, particle shape and the open areas throughout the microstructure. In addition, as the spherical form of the particles becomes less spherical, during compaction, the apparent density decreases as the friction surface area increases and the uniformity of the powder particle decreases.
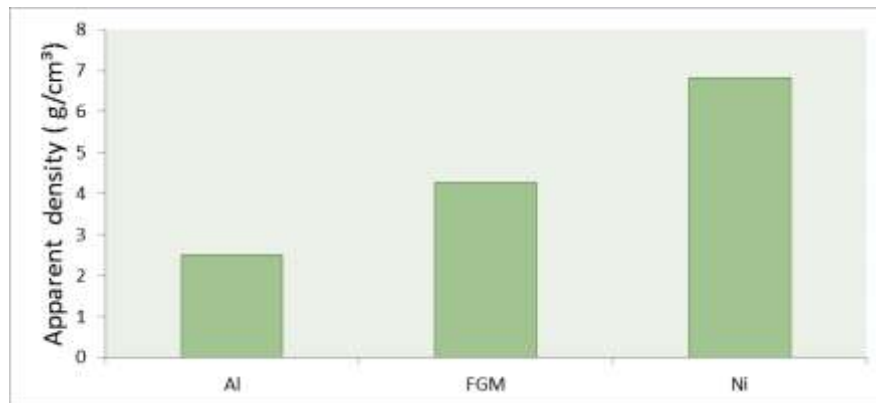
Figure 4. Apparent density of pure metal powder used in formation of FGM sample

Apparent densities of blended powders for (layer 1, layer 2, layer 3, layer 4, layer 5 and FGM) are shown in figure (5). Apparent density of layer 4 is the highest in comparison with the other layers, except layer 5, due to the high content of the higher atomic density (i.e. Ni). The measured apparent density of blended powders and the metal powders has been affected by the following parameters:
i. Loading rate and internal friction between particles in the same or different composition.
ii. Friction between particles and walls of baffle box and the small funnel.
Frictional forces between setting particles are reduced by decreasing surface area to volume ratios and decreasing surface roughness. As a result of this tendency, the apparent density is increased by allowing particles to transport more efficiently to fill the empty spaces between previously settled particles. Filling the spaces between particles with smaller particles is an efficient way to increase the apparent density of elemental or mixed powders.
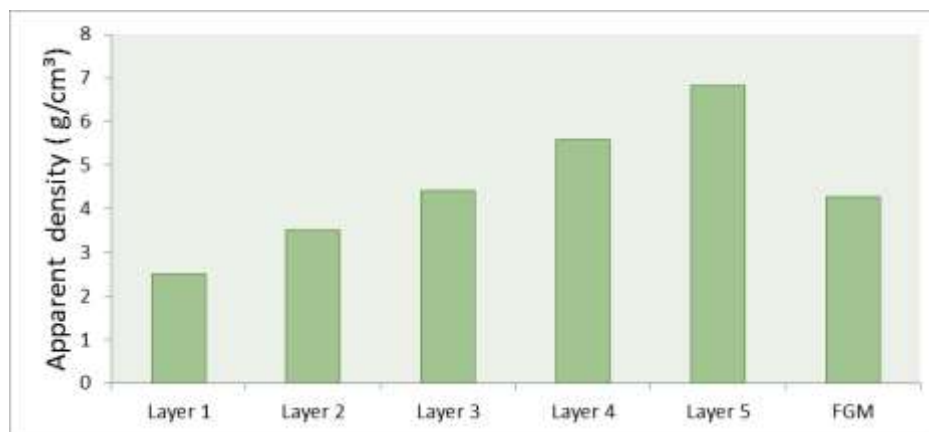

Figure 5. The apparent density of each layer and FGM before the sintering

3.3 Green density and Porosity of (Al/Ni FGM) compacts

Figure (6) depicts the green density of the prepared FGM as a function of compacting pressure. With rising pressing stress, the green density increases, from (300 MPa to 800 MPa). The powder particles are rearranged in the first step of compaction to partly remove bridging the stack of loose powder particles. Elastic and plastic deformation of the particles has occurred in the second step. The amount of plastic deformation is dependent on the ductility of the powder material that is the matrix aluminum powder here. Aluminum powder has much ductility than the Nickel powder. In the light of this statement, when plastic deformation of powder particles has been done, the powder particles are strain

hardened. In view of this statement, the powder particles are strain hardened when plastic deformation of powder particles has been performed. Fracture of powder particles that have been embrittled by work hardening is the third stage of compaction, under the increment of applied stress [11]. The density of compacts was measured using the mass (M) to volume (V) ratio (m). The changes in green density versus load are shown in Figure (6).
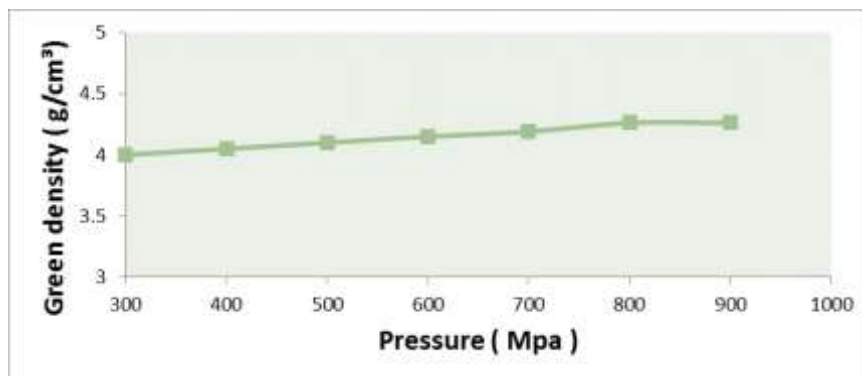

Figure 6. Green density of prepared FGMs samples as function of compacting pressure.

complementary of green density, the density of the powder mass increases with increasing of compacting pressure due to the amount of porosity in the mass decreases however, The size and distribution of pores will also differ [11].
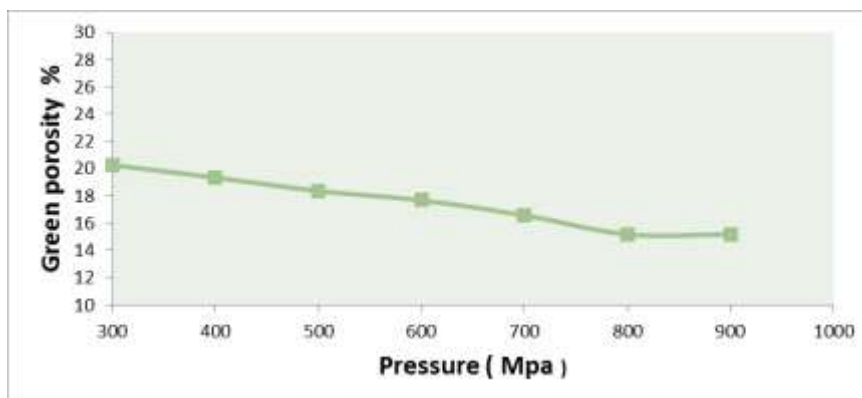

Figure 7. Green porosity percentages of FGMs samples as a function of compacting pressure.

3.4 Apparent density and porosity of sintered compacts
Sintering practices have crucial influences on most mechanical and physical properties of sintered compacts. Apparent density and porosity are affected by Sintering in noticeable manner. compacts under higher compacting pressure under sintering have traditional little pores than that at lower compacting pressure that lead in turn to an increment in apparent density. The figure (8) shows the apparent density of each layer and of functionally graded material (FGM). The variation of density between the different layers, shows an increase of density with the increasing the number of layers.
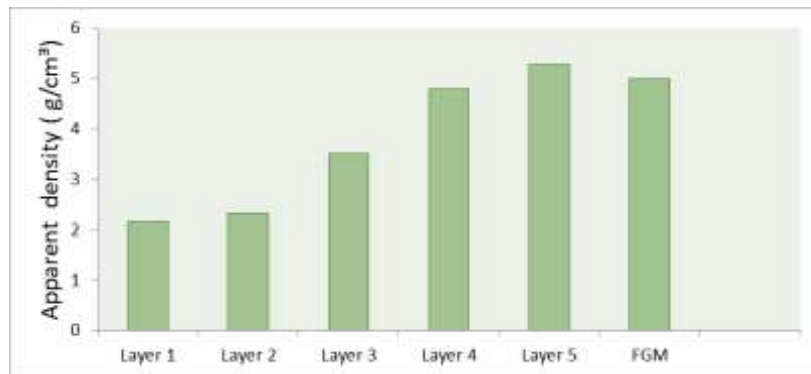
Figure 8. Apparent density of each layers and FGM sintered sample

Porosity is the complement of apparent density, so the shape of pores depends mainly on the temperature and time of sintering. Figure (9) shows the amount of the porosity after the sintering process. Compared with Figure (7), we note that there is a decrease in the amount of porosity after sintering than it was before sintering. The reason is that during the sintering process, diffusion of particles takes place, which leads to a decrease in the voids and an increase in the contact points between the particles. The highest amount of porosity was in layer 4 while the lowest amount was in layer 1.
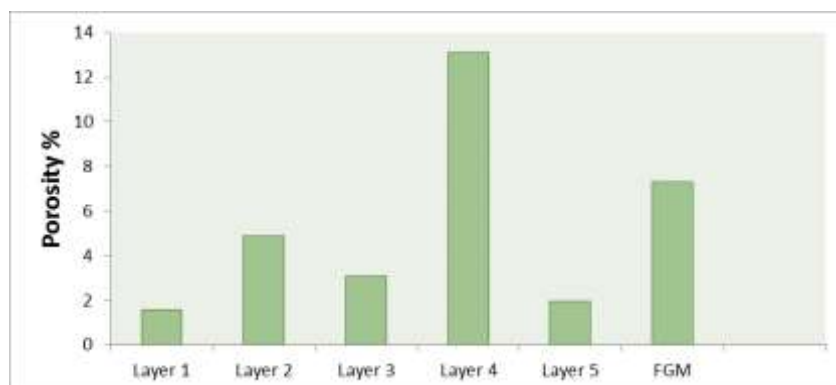

Figure 9. Porosity of each layer and FGM sintered sample

3.5 Lateral shrinkage of sintered compacts:

In this study, Al-Ni FGM is consist of a four-phase material consisting of Al particles, Al-Ni gradient, Ni particles (hard particles) and voids. The behavior of each phase is distinct, in which the porosity represented by void volume fraction, hard particles deform elastically and ductile metal particles deform elastoplastically. So the behavior of each phase is directly related to the shrinkage [14].

By diffusion, solid bonds are formed between the particles, which reduce the surface energy by reducing the intermediate space. Porosity is decreased when matrix particles sinter within themselves and around reinforcement particles. As sintering starts, sharp rise in porosity reduction are observed becouse of the nucleation of loosely packed particles. As sintering progresses, The consumption of porosity decreases because of the lack of small pores remaining to consume as well as the lack of energy to overcome the surface energy of the remaining large pore sizes [14]. Micro-stresses caused by matrix shrinkage can cause plastic deformation of the ductile metal phase, resulting in more porosity reductions. Changes in compact dimensions are essential considerations in the sintering process. The dimensional differences between green and sintered compacts parallel and/or

perpendicular to the direction of pressing is measured and expressed in percent of the green dimensions [15]. Figure (10) shows Shrinkage percentages of FGMs and of each layer.
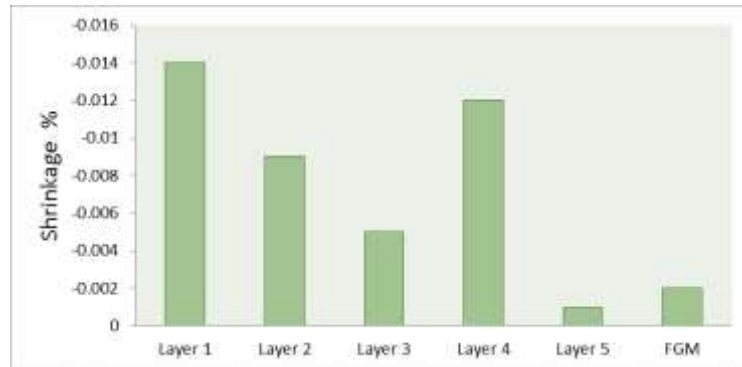

Figure 10. Shrinkage percentages of each layer and of FGMs

4. Conclusion

According to the current study, the following conclusions have been drawn: (i) by powder technology, aluminum and nickel functional gradient materials have been prepared and manufactured successfully under sintering temperature 600°C and 3 hours time. (ii) by modifying of apparent density of FGMs constituents in comparison with Al and Ni powder, better its circulation is achieved. (iii) high compaction pressure in parallel with the use of sintering temperature at (600 ℃) for (3 hrs.) can enhance the apparent density (3.99 g/cm³) and gives lower porosity percentage (7.3) in comparison with the other conditions. (iv) by Increasing of contact between functionally graded materials (FGMs) constituents leads to eliminate the pores. (v) although the sintering temperature that was used is (600 °C) compared to the melting point of nickel, we find that the nickel powder is well sintered.

References

[1]   U.Engel, B. Ilschner, Z. Werkstofftech. 17 (1986) 299-307.
[2]   N.Cherradi, A.Kawasaki, and M.Gasik, Compos. Eng. 4 (1994) No. 5, 883-894.
[3]   M.Gasik, Acta Polytech. Scand., Ch 226 (1995) 73 p.
[4]   M.Sasaki and T.Hirai, J. Ceram. Soc. Jap. 99 (1991) 970-980.
[5]   Koizumi M (1993) The concept of FGM. Ceram Trans Funct Grad Mater 34: 3-10.
[6]   D. Ravi, D.J. Green, Sintering stresses and distortion produced by density differences in bi-layer structures, Journal of the European Ceramic Society 26 (2006) 17–25.
[7]   S.E. Schoenberg, D.J. Green, A.E. Segall, G.L. Messing, A.S. Grader, P.M. Halleck, Stress and distortion due to green density gradients during densification, Journal of the American Ceramic Society 89 (10) (2006) 3027–3033.
[8]   T. Hirai, L. Chen, Recent and prospective development of functionally graded materials in Japan, Mater. Sci. Forum 308–311 (1999) 509–514.
[9]   Mandira Bhattacharyya, Amar Nath Kumar, Santosh Kapuria, Synthesis and characterization of Al/SiC and Ni/Al2O3 functionally graded materials, Materials Science and Engineering A 487 (2008) 524–535.

[10]   Vijay, Srinivasa RaoCH, A comparative investigation of hardness and compression strength of Nickel coated B4C reinforced 601AC/201AC selective layered functionally graded materials,2019,https://doi.org/10.1088/2053-1591/ab611a.

[11]   Ahmed Alaa Kandoh et al 2021 IOP Conf. Ser.: Earth Environ. Sci. 790 012073

[12]   Salam Hussein Ewaid et al 2021 IOP Conf. Ser.: Earth Environ. Sci. 722 012008

[13]   Abdul –Raheem Kadhim, "Investigation of Certain Shape Memory Alloys In Space Systems", Ph. D. Thesis, Materials Engineering, University of Babylon, 2007.

[14]   ASTM B - 328 Standard test method for density, Oil content, and interconnected porosity of sintered metal structural parts and oil – impregnated bearing, ASTM International, 2003.

[15]   Freeby, C.L. "Dimensional change of sintered metal compacts" in metals handbook 9th edition, powder metallurgy, Vol.7, p. (290), 1984.

[16]   Nawal M. Dawood, "Preparation & Characterization of Coated & Cu alloyed Bio Nitinol", Ph.D. thesis, University of Technology, Department of Materials Engineering, Baghdad, 2014.

[17]   Salam Hussein Ewaid et al 2021 IOP Conf. Ser.: Earth Environ. Sci. 790 012075

[18]   Burak ÖZKAL, Anish UPADHYAYA, M.L. ÖVEÇO□LU and Randall M. GERMAN, "Realtime Sintering Observations in W-Cu system: Accelerated Rearrangement Densification via Copper Coated Tungsten Powders Approach", Euro PM Sintering, 2004.

[19]   Chong, F. L., Chen, J. L., Zhou, Z. J., and Li, J. G., "fabrication and plasma exposure of fine-grained tungsten / copper functionally graded materials in the HT-7 tokamak", Fusion Science and Technology, Vol. 53, p.p. (1-6), 2008.

[20]   Yousif, R., & Hayat Adil Ali. (2020). Temperature-Dependent Viscosity Effect on the Peristaltic Transport of (MHD) blood flow Ree-Eyring Fluid Through Porous Medium in an Inclined Asymmetric Channel. Al-Qadisiyah Journal Of Pure Science, 25(3), math 16-34.

[21]   Raad Aziz Hussan Al-Abdulla, & . Othman Rhaif Madlooi Al-Chrani. (2020). On Semi Feebly Open Set and its Properties. Al-Qadisiyah Journal Of Pure Science, 25(3), math 35-45.